Journal of Hazardous Materials 185 (2011) 77–85

Contents lists available at ScienceDirect

Journal of Hazardous Materials

journal homepage: www.elsevier.com/locate/jhazmat

# Photodegradation of methyl orange by photocatalyst of CNTs/P-$TiO_2$ under UV and visible-light irradiation

Shaohua Wang[a,b], Shaoqi Zhou[a,c,d,e,*]

[a] School of Environmental Science and Engineering, South China University of Technology, Guangzhou 510006, PR China
[b] School of Chemistry and Chemical Engineering, Guangdong Pharmaceutical University, Zhongshan 528458, PR China
[c] State Key Laboratory of Subtropical Building Science, South China University of Technology, Guangzhou 510641, PR China
[d] Key Laboratory of Environmental protection and Eco-Remediation of Guangdong Regular Higher Education Institutions, South China University of Technology, Guangzhou 510006, PR China
[e] Key Laboratory of Pollution Control and Ecosystem Restoration in Industry Clusters, South China University of Technology, Guangzhou 510006, PR China

ARTICLE INFO

*Article history:*
Received 4 May 2010
Received in revised form 20 July 2010
Accepted 31 August 2010
Available online 9 September 2010

*Keywords:*
Photocatalyst
P-doped
$TiO_2$
Carbon nanotubes
Hydrothermal

ABSTRACT

A novel nanoscale photocatalyst CNTs/P-$TiO_2$ was successfully prepared by hydrothermal method. The morphology and the physicochemical properties of the prepared samples were investigated using TEM, XPS, XRD, BET, FTIR, TG-DSC and UV–vis DRS spectroscopy. The photocatalytic activity was evaluated by degradation of methyl orange (MO) dye. The results demonstrated that CNTs/P-$TiO_2$ nanoparticles could effectively photodegrade MO not only under UV irradiation but also under visible-light (VL) irradiation. The MO degradation performance on CNTs/P-$TiO_2$ was superior to that of the commercial P25. The optimal mass ratio of CNTs to P-$TiO_2$ in the nanocomposite catalyst was 5:100. The synergetic effect was discussed in terms of different roles played by phosphorus doping and introducing CNTs into the composite catalysts.



## 1. Introduction

Since the discovery of photocatalytic splitting of water on $TiO_2$ electrodes by Fujishima and Honda in 1972 [1], heterogeneous photocatalysis by semiconductors has attracted much interest due to its applications in environmental purification and solar energy conversion [2]. It especially provides an economical and ecological method for the remediation of contaminated water and air [3,4]. Among various semiconductor materials widely used in photocatalysis, $TiO_2$ has proved to be the most suitable one because of its many desirable properties such as high activity, chemical stability, robustness against photocorrosion, low toxicity, no secondary pollution, low cost and water insolubility under most conditions [5].

However, many problems remain unresolved in $TiO_2$ photocatalytic system for practical applications, such as low photon utilization efficiency and narrow spectrum responsive range ($\lambda < 388$ nm). Several methods have been applied to improve the photocatalytic efficiency of $TiO_2$. Doping with non-metals, such as N, P, B, C, S, F, Cl and Br, has been widely used for the modification of $TiO_2$ to improve its photocatalytic activity or to extend its light absorption into the visible region [6–15]. Among them, the phosphorous-doped $TiO_2$ has recently attracted increasing interest due to its enhanced photocatalytic efficiency [16–25]. Compared with pure $TiO_2$, the as-prepared P-doped $TiO_2$ shows a narrower band gap. In addition, it has an absorption tail in the visible-light region. Consequently, it is more effective in the photocatalytic degradation of organic contaminants under visible-light irradiation. Shi et al. [19] found that P-doped $TiO_2$ prepared by a sol–gel method with $NaH_2PO_4$ as precursor demonstrated a higher photocatalytic activity under visible-light irradiation than pure $TiO_2$. Ozaki et al. [22] prepared $TiO_2$ modified with various elements and investigated the physical and photocatalytic properties of the samples. They found that phosphorus was the most effective dopant for photocatalytic decomposition of acetaldehyde under visible-light irradiation. Zhu and co-workers [25] synthesized the P-doped $TiO_2$ with high crystallinity and large surface area by hydrothermal method. The methylene blue degradation performance on the P-doped $TiO_2$ was significantly enhanced and superior to that of the commercial P25.

Another approach for enhancing the photocatalytic efficiency of $TiO_2$ involves adding a co-adsorbent such as activated carbon (AC) [26–28], graphite [29,30], and carbon nanotubes (CNTs) [31,32].

*Abbreviations:* MWCNTs, Multi-walled carbon nanotubes; MO, methyl orange; VL, visible-light; PT, P-$TiO_2$; CPTCNTs/P-, $TiO_2$; CPT005, CNTs/P-$TiO_2$ with the mass ratio of CNTs to P-$TiO_2$ being 0.05; CPT010, CNTs/P-$TiO_2$ with the mass ratio of CNTs to P-$TiO_2$ being 0.10; CPT020, CNTs/P-$TiO_2$ with the mass ratio of CNTs to P-$TiO_2$ being 0.20.

* Corresponding author at: School of Environmental Science and Engineering, South China University of Technology, Guangzhou 510006, PR China.
Tel.: +86 20 39380579; fax: +86 20 85511266.
*E-mail address:* fesqzhou@scut.edu.cn (S. Zhou).

0304-3894/$ – see front matter © 2010 Published by Elsevier B.V.
doi:10.1016/j.jhazmat.2010.08.125

It has been reported that the presence of carbon materials in $TiO_2$ photocatalysts can also induce some beneficial effects on their photocatalytic activities [11,33]. Faria and Wang [34] reviewed the application of various carbon materials in photocatalysis during the last decade. Recently, CNTs have been regarded as more attractive catalyst supports than activated carbons because of their combination of electronic, adsorption, mechanical and thermal properties [35]. CNTs can conduct electrons, and have strong adsorption and specific semiconducting characteristics. CNTs/$TiO_2$ composite catalysts have been successfully prepared by various processes [36–40]. The studies on CNTs/$TiO_2$ reveal a considerable synergy effect with metal oxides and carbon phases. Furthermore, researchers have shown that CNTs can increase the adsorption and photocatalytic activity of $TiO_2$ in the presence of UV and VL irradiation. Therefore, CNTs can be used as a promising material for environmental cleaning, and can be adopted to improve the photocatalytic efficiency of $TiO_2$.

Our work aims to synthesize a composite photocatalyst with higher photocatalytic activity and wider spectrum responsive range than pure $TiO_2$. In this study, the nanocatalysts of CNTs/P-$TiO_2$ (labeled as CPT) with varying mass ratios of CNTs to P-$TiO_2$ were synthesized by hydrothermal method. The influence of phosphorus and CNTs on the structural behavior of the $TiO_2$ samples was studied by XPS, XRD, BET, TEM, UV–vis DRS. The photocatalytic degradation of methyl orange (MO) dye under UV and VL irradiation was investigated over nanosized CNTs/P-$TiO_2$ photocatalysts.

## 2. Experimental

### 2.1. Materials

Multi-walled carbon nanotubes (MWCNTs), 10–20 nm in diameter and 5–15 μm in length, were purchased from Shenzhen Nanotech Port Co., Ltd., China. Titanium (IV) *n*-butoxide ($Ti(OBu)_4$, 98%) was chosen as a Ti precursor, which was chemical pure grade. P25 $TiO_2$ (ca. 80% anatase, 20% rutile) was obtained from the Degussa AG Company in Germany. MO was analytical grade reagent from Tianjin Tianxin Fine Chemical Development Center in China and used without further purification. Distilled water was additionally cleaned prior to its use with a quartz sub-boil high purity water purification system. All other chemical reagents were analytical grade.

### 2.2. Acid treatment of CNTs

Acid treatment of CNTs was used to get oxygenated functionalities on the nanotube surfaces. This improved the combination of CNTs with $TiO_2$. The treatment could also lead to the opening of the ends and/or breakage of the tubes and removal of the amorphous carbon and metal catalyst [41].

In a typical acid treatment, 1 g pristine CNTs were immersed into a 40 mL mixed solution of concentrated sulphuric acid and nitric acid with a volume ratio of 3:1 [42,43]. The mixture was then heated to 140 °C (its boiling point) for 20 min under refluxing and cooled naturally to room temperature. The CNTs were filtered and washed with distilled water until the pH of the filtered solution was about 6–7. The product was then dried at 80 °C in an oven and kept in a desiccator for further use.

### 2.3. Preparation

For preparation of CNTs/P-$TiO_2$, 5.01 g tetrabutyl titanate was dissolved in 25 mL ethanol, followed by the addition of certain amounts of CNTs, and then this solution was sonicated for 30 min. After that, 10 mL hypophosphorous acid solution was added dropwise to the above solution under vigorous stirring. The P/$TiO_2$ molar ratio in the resulting suspension was 0.02. After stirring for 2 h, the mixture was transferred to a 50 mL Teflon-lined stainless steel autoclave, followed by a hydrothermal treatment at 260 °C for 24 h. After cooling down, the powder sample was filtered, rinsed with ethanol and distilled water, and dried at 110 °C for 12 h. The mass ratio of CNTs to P-$TiO_2$ in the obtained samples was 0.05, 0.10 and 0.20, which were denoted as CPT005, CPT010 and CPT020, respectively. P-$TiO_2$ without CNTs was denoted as PT. Pure $TiO_2$ without phosphorous doping was similarly prepared except that tetrabutyl titanate was hydrolyzed in pure water.

### 2.4. Characterization

The bare CNTs and the prepared samples were characterized by a range of analytical techniques. The XRD patterns with diffraction intensity vs. $2\theta$ were recorded in a X-ray diffractometer (XRD, D8 ADVANCE, Bruker, Germany) using graphite monochromatic copper radiation (Cu-Kα, $\lambda = 0.15418$ nm) at 40 kV, 40 mA over the $2\theta$ range 10–90° at room temperature. The morphology and microstructure of the samples were characterized with a scanning electron microscopy (SEM, JSM-6380LA, JEOL, Japan) equipped with an energy dispersive X-ray spectrometer (EDS, Inca 300, Oxford Instruments, U.K.) and a transmission electron microscope (TEM, JEM-100CXII, JEOL, Japan). The specimens for TEM were prepared by dispersing the final powders in ethanol with 20 min ultrasonication and placing a drop of this mixture on carbon-copper grids. X-ray photoelectron spectroscopy (XPS) measurements were performed on a Kratos Axis Ultra-DLD System with monochromatic Mg Kα X-rays (1253.6 eV) operated at 15 V and 15 mA (emission current) in a chamber with a base pressure of approximately $10^{-8}$ Pa. The adsorption–desorption isotherms of $N_2$ at 77 K were measured with an adsorption instrument (TriStar II, Micromeritics Company, USA) to evaluate their pore structures. All samples were degassed at 180 °C before the measurements. The specific surface areas were determined using BET Equation and the pore size distributions were analysed using the BJH method. Thermogravimetric and differential scanning calorimetry analyses (TG-DSC) were performed by a thermal analysis instrument (STA 449C, NETZSCH, Germany) from room temperature to 850 °C at a temperature-ramping rate of 10 °C $min^{-1}$ in an air flow of 50 mL $min^{-1}$. Fourier transform infrared spectra (FTIR) of the samples were recorded in a Fourier transform infrared spectrometer (Nicolet 6700, Thermo NICOLET Company, USA) using pellets of KBr. Optical absorption spectra (UV–vis DRS) of the solid materials were recorded over the range of 190–800 nm in the absorption mode using a UV–vis spectrophotometer (UV-3010, Hitachi Ltd., Japan) equipped with an integrating sphere attachment. $BaSO_4$ was employed as a reference substance.

### 2.5. Photocatalytic studies

The photocatalytic activity of the samples was studied by the degradation of MO dye as a target pollutant. The photocatalytic reaction system included a 500 mL cylindrical glass reactor equipped with a light source, which was located axially and held in a quartz immersion tube. A circulating water jacket was employed to cool the radiation source and cancel the infrared radiation, thus preventing any heating of the suspension. Air was bubbled through the reaction solution from the bottom with an air flow of 0.6 L $min^{-1}$ to ensure effective dispersion and a constant dissolved $O_2$ concentration.

In a typical photocatalytic test performed at room temperature, 0.1 g photocatalyst was added into 250 mL MO aqueous solution with a concentration of 20 mg $L^{-1}$, and then dispersed by ultrasonic treatment for 10 min. The suspension was stirred in the dark for 30 min to reach the adsorption–desorption equilibrium before the irradiation started. UV and VL irradiation was provided by a 250 W

high-pressure mercury lamp and a 400 W halogen-tungsten lamp with a light filter to cut off the light below 410 nm. After a defined time interval, 5 mL suspension was sampled and centrifuged. Then the changes of MO concentration were monitored using a UV–vis spectrophotometer (U-3010, Hitachi, Japan). Pure $TiO_2$ and Commercial P25 were used for comparison. The MO removal under UV and VL irradiation without catalyst was also carried out to observe the light irradiation effect on the MO degradation.

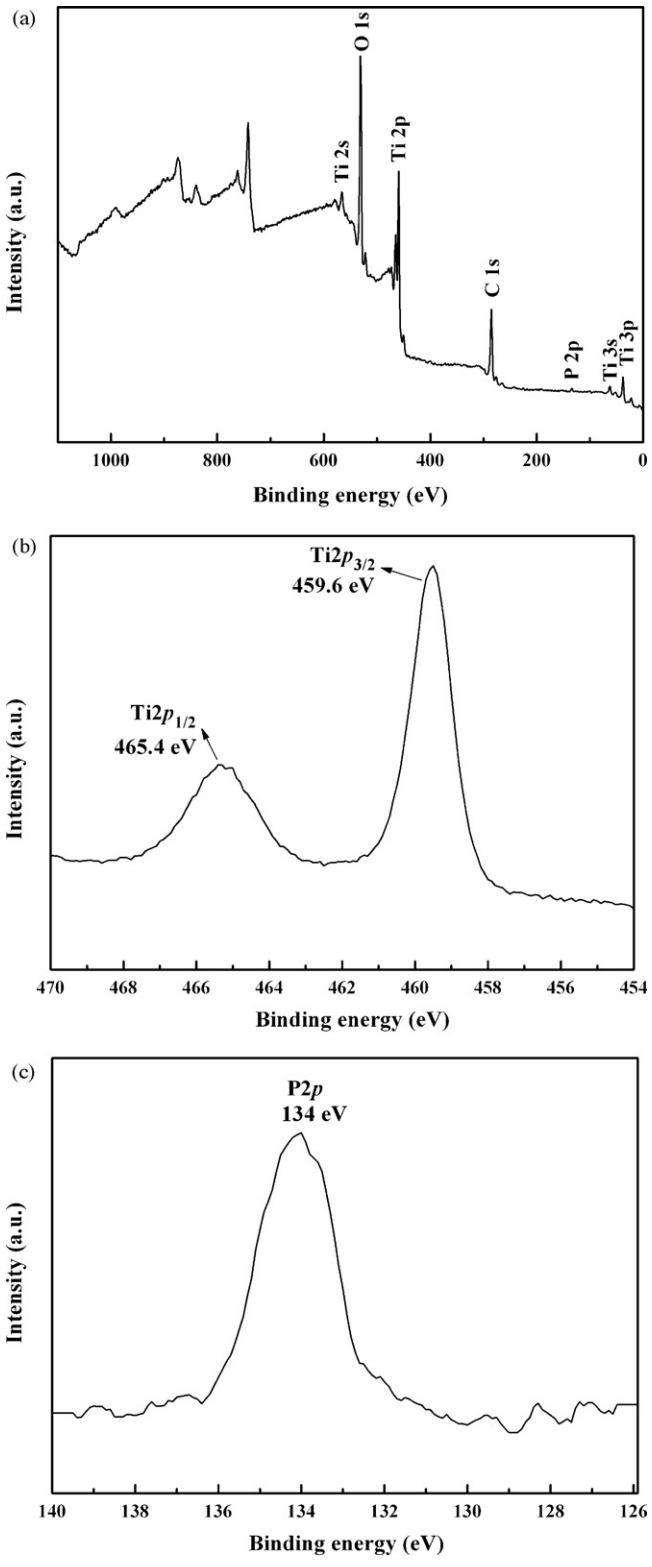


**Fig. 1.** (a) XPS survey spectrum, (b) High-resolution XPS spectra of Ti 2p and (c) High-resolution XPS spectra of P 2p region of CPT005.

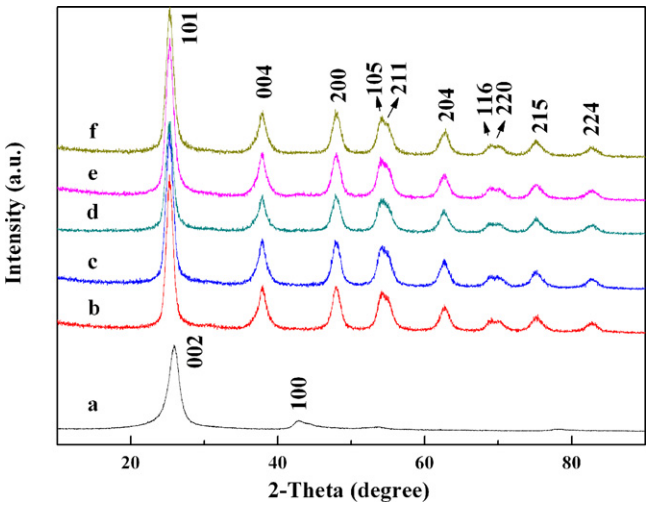


**Fig. 2.** XRD patterns of (a) CNTs, (b) $TiO_2$, (c) PT, (d) CPT005, (e) CPT010, (f) CPT020.

## 3. Results and discussion

### 3.1. XPS analysis

The chemical forms of surface elements in the CNTs/P-$TiO_2$ sample were investigated by XPS analysis. The XPS survey spectrum of the CPT005 sample is shown in Fig. 1(a). The characteristic energy spectrum of four kinds of atoms, titanium, oxygen, carbon and phosphorus can be observed. The photoelectron peak for Ti 2p appeares clearly at a binding energy, $E_b$, of 459 eV, with O 1s at $E_b$ = 531 eV, C 1s at $E_b$ = 285 eV and P 2p at $E_b$ = 134 eV. The C 1s peak corresponds to the CNTs, while the Ti 2p and O 1s peaks can be attributed to $Ti^{4+}$ and $O^{2-}$.

Fig. 1(b) displays the XPS spectrum of Ti 2p for CPT005. The XPS peaks in the Ti 2p region appear at 459.6 (Ti $2p_{3/2}$) eV and 465.4 (Ti $2p_{1/2}$) eV, slightly shifting toward higher binding energy compared with those of the pure bulk anatase $TiO_2$ [44]. This suggests that the chemical bond of the Ti atom in CPT005 is different from that in the pure anatase $TiO_2$. The more electronegative $P^{5+}$ atom replaces the $Ti^{4+}$ atom in the surface or near surface region, pulling the electrons in Ti–O bond a bit away from Ti atom, thus causing a little rise of the Ti $2p_{3/2}$ binding energy. It was evaluated that the $P^{5+}$ replaced a part of $Ti^{4+}$ in the crystal lattice of $TiO_2$, which resulted in the charge imbalance [45] and decreased the recombination rate of photogenerated electrons and holes. The peaks of 455 eV assigned to $Ti^{2+}$ (TiO) and 456.7 eV assigned to $Ti^{3+}$ ($Ti_2O_3$) were not observed. Therefore, it can be concluded that only titanium dioxide existed.

Fig. 1(c) shows the high-resolution XPS spectrum of P in the CPT005 sample. There is only one peak at 134 eV in the P 2p XPS spectrum, indicating that P ions are in the pentavalent-oxidation state ($P^{5+}$). The existence of Ti-P bonds in the CPT005 sample can be excluded because the characteristic peak of P in Ti–P at around 128 eV was not observed.

### 3.2. XRD analysis

To characterize the crystalline structure of the samples, the XRD patterns of pristine CNTs, P-$TiO_2$ and CNTs/P-$TiO_2$ composites (Fig. 2) are obtained. Fig. 2(a) shows the XRD patterns of the pristine CNTs. The peaks centered at 25.9° and 42.9° correspond to the (0 0 2) and (1 0 0) reflections of the graphite from the CNTs.

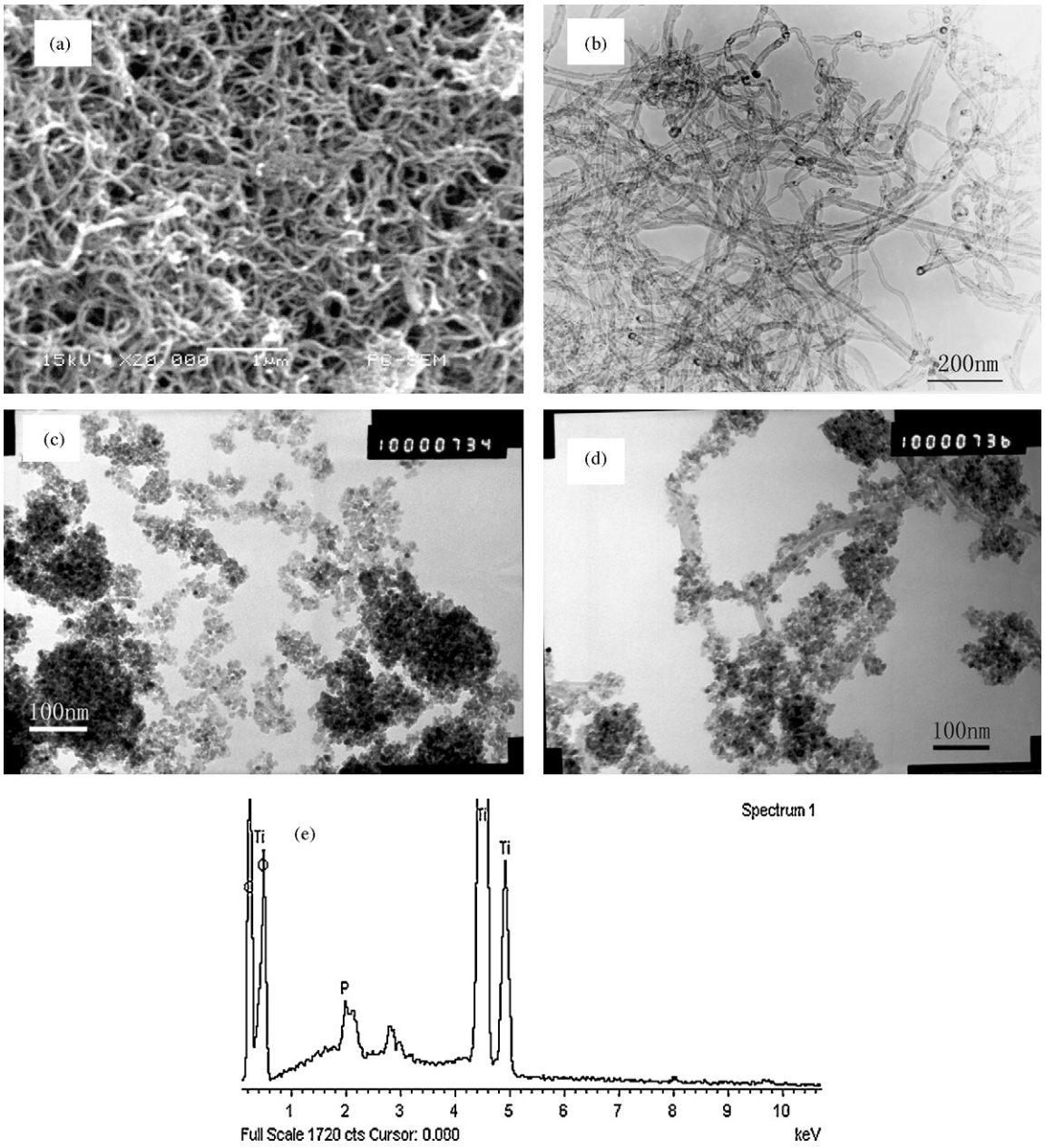


**Fig. 3.** (a) SEM image of CNTs, (b) TEM image of CNTs, (c) TEM image of PT, (d) TEM image of CPT005 and (e) EDS spectrum of the coating layer of P-$TiO_2$ on CNTs.

For $TiO_2$ and composite catalysts, all the sharp peaks observed in the XRD patterns belong to the anatase phase of $TiO_2$ (JCPDS no. 21-1272). It is noteworthy that the characteristic peaks of the CNTs can hardly been identified from all the patterns of the composite catalysts. The reason may be that the main peak of CNTs at 25.9° is overlapped with the main peak of anatase $TiO_2$ at 25.4°.

In general, the full width at half-maximum of XRD peak is related to the particle size of crystal materials. The mean crystallite size can be calculated from full-width at half-maxima of the (2 0 0) peak (not being interfered by CNTs) of the anatase by Debye–Scherrer formula:

$$D = \frac{K\lambda}{\beta\cos\theta} \quad (1)$$

where $\lambda$ is the wavelength corresponding to the Cu K$\alpha$ irradiation ($\lambda = 0.15418$), $K$ is the Scherrer constant ($K = 0.89$), $\theta$ is the diffraction angle and $\beta$ is the full width at half-maximum [46]. $TiO_2$ crystallite size ($d_{TiO_2}$) estimated from the line broadening by Scherrer's equation is compared in Table 1. A crystallite size for pure $TiO_2$ of 7.1 nm is calculated while the size decreases to 6.6 nm, 6.6 nm, 6.5 nm and 6.4 nm for PT, CPT020, CPT010 and CPT005, respectively. It is seen that the crystallite size decreased after doping with phosphorus, suggesting that the P-doping could efficiently inhibit the growth of $TiO_2$ nanocrystallites.

### 3.3. Microscopy study

As shown in Fig. 3(a) and (b), the CNTs have an average diameter of 10–20 nm and lengths ranging from hundreds of nanometers to micrometers. The individual nanotubes display a hollow structure without any remarkable amorphous carbon.

Fig. 3(c) and (d) show the typical TEM images of the prepared PT and CNTs/P-$TiO_2$ nanoparticles. The P-$TiO_2$ particles are spherical. A few aggregates of P-$TiO_2$ nanocrystallites can be observed due to the high temperature and pressure in the hydrothermal system. In Fig. 3(d), the CNTs are surrounded by P-$TiO_2$ nanocrystals. Most

**Table 1**
Carbon content ($C_{PV}$, $C_{TG}$), BET surface area ($S_{BET}$), total pore volume ($V_p$), average pore diameter ($D_p$) and $TiO_2$ crystal size ($d_{TiO_2}$) of samples.

| Samples | $C_{PV}$ (wt%)[a] | $C_{TG}$ (wt%)[b] | $S_{BET}$ ($m^2\ g^{-1}$) | $V_p$ ($cm^3\ g^{-1}$)[c] | $D_p$ (nm) | $d_{TiO_2}$ (nm)[d] |
|---|---|---|---|---|---|---|
| CNTs | 100 | >98 | 109.04 | 0.60 | 22.10 | – |
| $TiO_2$ | – | – | 61.82 | 0.56 | 17.2 | 7.1 |
| PT | – | – | 156.52 | 0.33 | 8.37 | 6.6 |
| CPT005 | 4.76 | 4.81 | 163.09 | 0.32 | 7.89 | 6.4 |
| CPT010 | 9.09 | 8.96 | 165.07 | 0.33 | 7.92 | 6.5 |
| CPT020 | 16.67 | 16.83 | 162.76 | 0.40 | 9.80 | 6.6 |

[a] The carbon content in the nanocomposite catalysts corresponded to the predetermined value before sample preparation.
[b] The carbon content in the nanocomposite catalysts was measured by TG-DSC analysis.
[c] The total pore volume was evaluated for a $P/P_0$ ratio of 0.99.
[d] $TiO_2$ crystal size was calculated by Scherrer's equation (applicable from 1 nm to 100 nm).

of the CNTs including individual CNTs and CNT clusters are coated with P-$TiO_2$ nanoparticle layers. This indicates the intimate conjugation effect between CNTs and P-$TiO_2$. A few segregated P-$TiO_2$ nanoparticles aggregate along the P-$TiO_2$ coating layers.

EDS is carried out to probe the composition of the attached nanoparticles. The spectrum is shown in Fig. 3(e). It reveals the presence of Ti, O, P, and C on the surface of the CNTs. This is consistent with the results of XPS. It also confirms the coating of P-$TiO_2$ nanoparticles on CNTs.

### 3.4. TG-DSC analysis

TG-DSC analysis was carried out to estimate the carbon nanotubes contents of the composites. The TG-DSC curves for the thermal decomposition of P-$TiO_2$, purified CNTs, and CPT005 are shown in Fig. 4. It is found that there is only a slight weight loss of P-$TiO_2$ (about 3.7%) attributed to the loss of adsorbed water and ethanol. For the purified CNTs, the initial burning temperature is about 600 °C, and there is only one sharp exothermic peak around 672 °C in the DSC curve. Kim et al. [47] reported temperature of 500–700 °C as the oxidation temperature for CNTs. The result shows the high purity of the CNTs. Otherwise there would be signals between 300 °C and 400 °C associated with amorphous carbon. In Fig. 4(b), the weight loss of the CPT005 sample in the range of 550–690 °C is due to oxidation of carbon nanotubes. There is one sharp exothermic peak around 644 °C in the DSC curve. The shift of exothermic peak compared with CNTs may be ascribed to the presence of the metal oxide deposited on the sidewall of CNTs which facilitates oxidation of carbon species. In the composite CPT005, the content of CNTs is 4.81% measured by TG method. The CNTs contents of the composites estimated from TG-DSC analysis are listed in Table 1. The results suggest that the CNTs contents obtained from TG-DSC analysis are in good agreement with the predetermined values before sample preparation. Therefore, the losses of CNTs during the preparation procedure are negligible.

### 3.5. BET surface area and pore properties measurements

The $N_2$ adsorption–desorption isotherms and the pore size distribution for purified CNTs, PT, and CPT composites are shown in Fig. 5. The BET surface area, pore volumes and average pore diameters are also listed in Table 1. All the isotherms can be ascribed to type IV, indicating the presence of a mesoporous pore structure. The pore size distribution plot of the purified CNTs exhibits a wide pore size distribution ranging from 5 nm to 100 nm. PT presents monomodal pore size distribution centered at 8.37 nm. When CNTs are composited with P-$TiO_2$, the pore size distributions of the composites become narrow. The high distribution centers at 7.88 nm, 7.92 nm and 9.80 nm can be attributed to P-$TiO_2$, while the pores bigger than 15 nm in CNTs are obviously reduced for all the composite catalysts. The reduction in pore volume of the composites compared to the acid treated CNTs strongly suggests that the deposited P-$TiO_2$ particles could block the CNTs pores. It is interesting to note that the $S_{BET}$ of PT is increased significantly compared with that of $TiO_2$. Moreover, the $S_{BET}$ of the composite catalysts are higher than that of the acid treated CNTs and PT particles.

### 3.6. FTIR analysis

FTIR spectra of prepared samples are presented in Fig. 6. The broad peak at 3410 $cm^{-1}$ and the peak at 1630 $cm^{-1}$ are assigned to –OH stretching and bending vibrations, respectively. The peak at 600 $cm^{-1}$ is assigned to the Ti–O stretching vibration. In addition, an absorption peak at 1040 $cm^{-1}$ in PT spectra is the characteris-

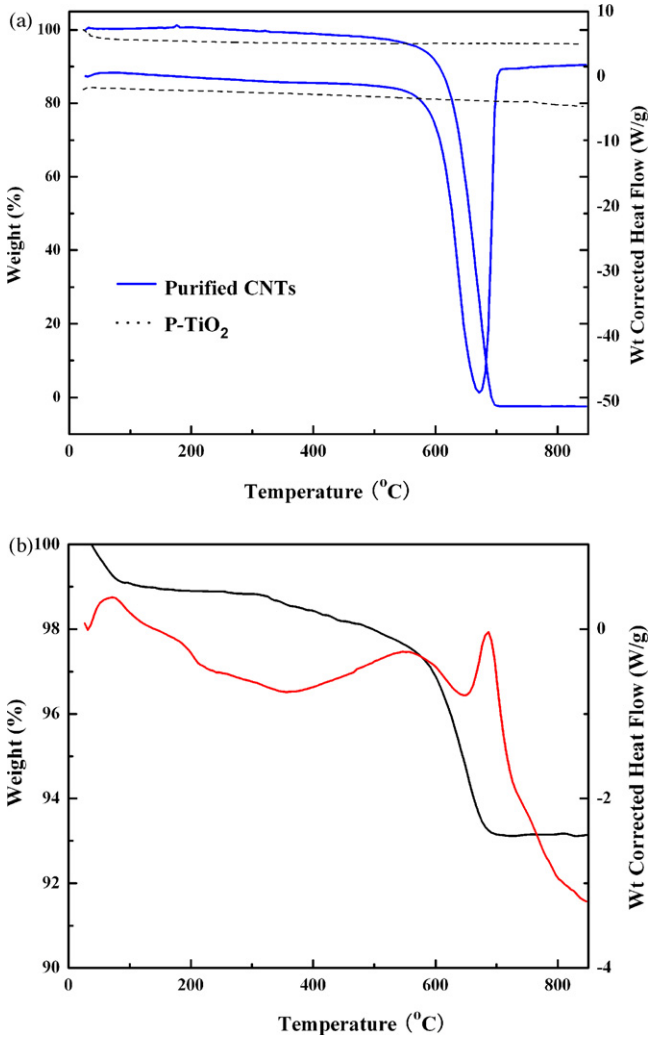


**Fig. 4.** TG-DSC curves of (a) CNTs and P-$TiO_2$, (b) CPT005.

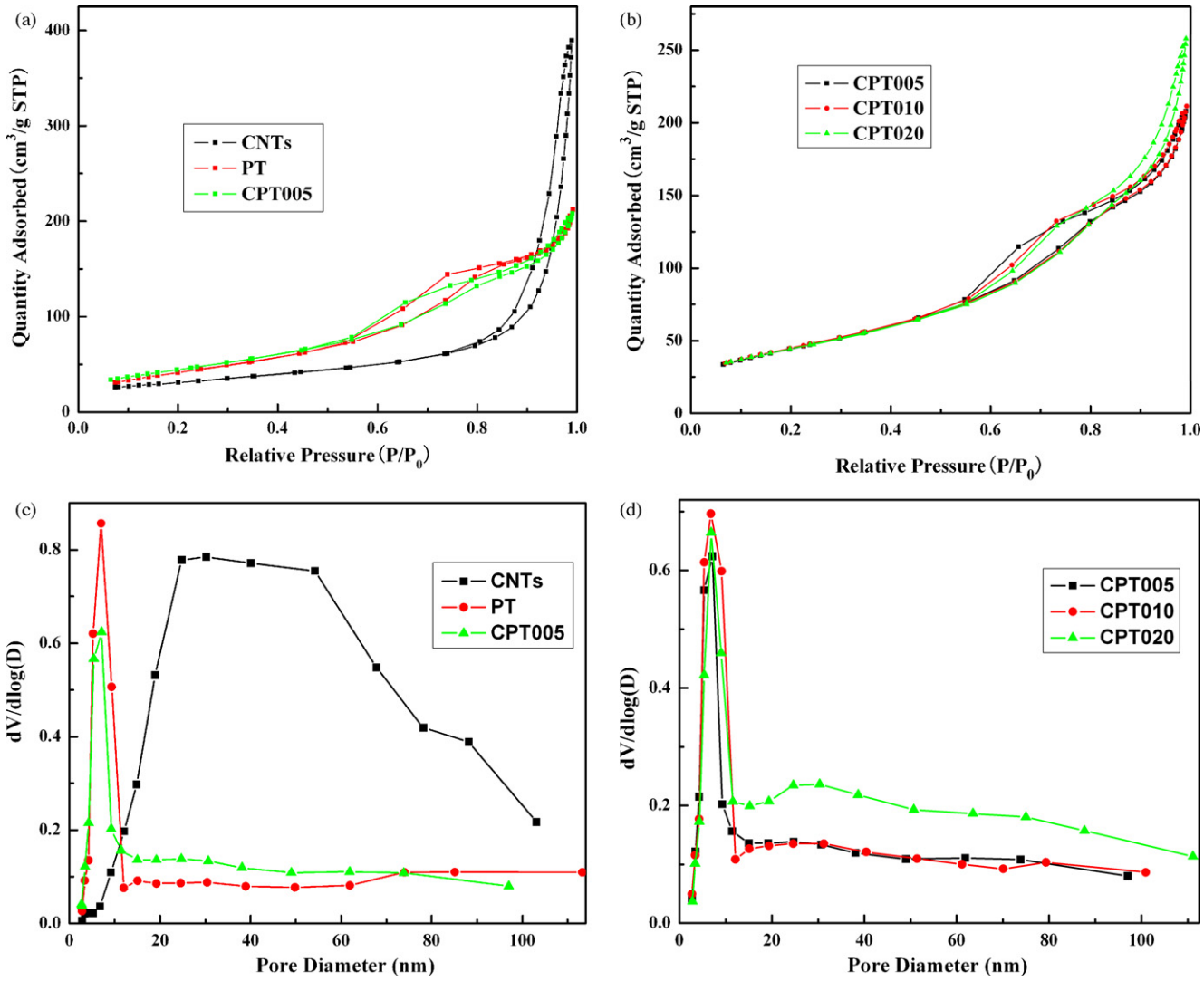


**Fig. 5.** (a) and (b) $N_2$ adsorption–desorption isotherms and (c) and (d) pore size distribution of samples.

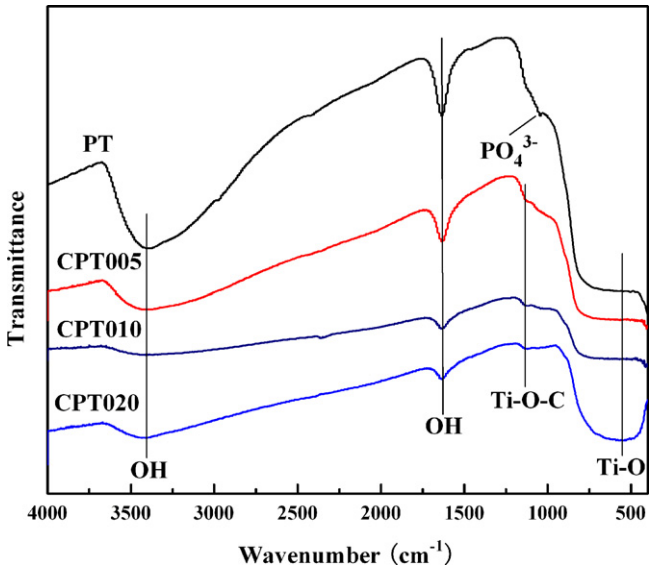


**Fig. 6.** FTIR spectra of PT and CNTs/P-$TiO_2$ composites.

tic frequency of $PO_4^{3-}$. However, another characteristic frequency of $PO_4^{3-}$, phosphoryl (P=O) at 1300–1400 $cm^{-1}$ cannot be found. Therefore, the phosphorus might exist not simply in the form of $PO_4^{3-}$ but probably in the form of Ti–O–P bond. It is noteworthy that a new peak at 1100 $cm^{-1}$ appears after P-$TiO_2$ is immobilized on CNTs. The typical peak at 1100 $cm^{-1}$ should be attributed to a newly formed Ti–O–C bond, indicating an evident conjugation effect between CNTs and Ti–O bonds. Thus, P-$TiO_2$ adheres to the CNTs surface by C–O–Ti bonding and is interconnected by Ti–O–Ti bonding. The result is the encapsulation of P-$TiO_2$ particles onto CNTs.

### 3.7. UV–vis DRS analysis

Fig. 7 shows the UV–vis DRS spectra of pure $TiO_2$, PT, CNTs and CNTs/P-$TiO_2$ composites. CNTs have a broad absorption area. It is noticeable that there is an obvious correlation between the contents of CNTs and the UV–vis DRS spectrum change, and adsorption increases with increasing CNTs content of the composite catalysts. Furthermore, the absorption even covers the whole range of the measured UV–vis region due to the introduction of CNTs. This indicates that the deposition of CNTs is good for the light-absorbing properties of the composites. The absorption threshold of pure titania is 385 nm. It presents a strong absorption band only in the UV

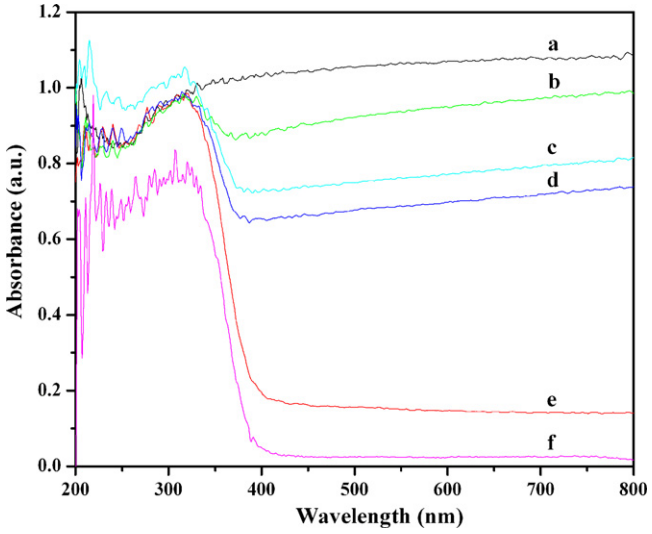


**Fig. 7.** UV–vis DRS spectra of (a) CNTs, (b) CPT020, (c) CPT010, (d) CPT005, (e) PT and (f) $TiO_2$.

region which is attributed to the band-band transition. However, all CNTs/P-$TiO_2$ samples exhibit extended absorption range to the visible region, and yield a large red shift compared to pure $TiO_2$. Thus, the photocatalytic activity could be enhanced under visible illumination. Moreover, in the UV region, a little increase in the absorption intensity of CNTs/P-$TiO_2$ samples is observed. Yang et al. [48] calculated the electronic structure of P cation-doped anatase titania and found that the replacement of P cation ($P^{5+}$) to $Ti^{4+}$ led to a slight rise of the valence band, thus causing a tiny narrowing of the band gap. This theoretical result accords fully with our experimental conclusion. The absorption features suggest that the prepared CNTs/P-$TiO_2$ photocatalyst should be responsive to the visible-light.

### 3.8. Photocatalytic activity

Photodegradation of MO under UV and visible-light irradiation is employed to evaluate the photocatalytic activity of the prepared catalysts. Fig. 8 shows the changes in the absorbance profiles of MO solution in the presence of CPT005 under UV irradiation. Two characteristic peaks (271 nm, 463 nm) are observed, and maximum absorption occurs at 463 nm. With the irradiation time increasing, the peaks at 271 nm and 463 nm reduced quickly. The band at 463 nm became very weak and disappeared in 80 min, suggesting almost complete degradation of MO. The absorption peaks show a slight blue shift during the course of the photodegradation.

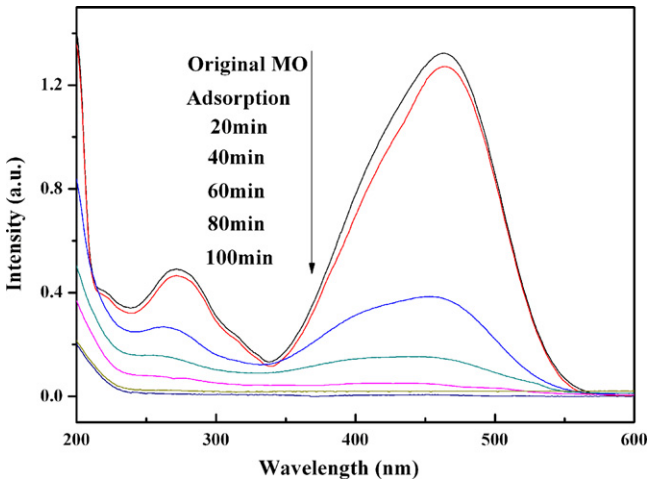


**Fig. 8.** Variations of the UV–vis absorption spectra of MO solution by CPT005 under UV irradiation.

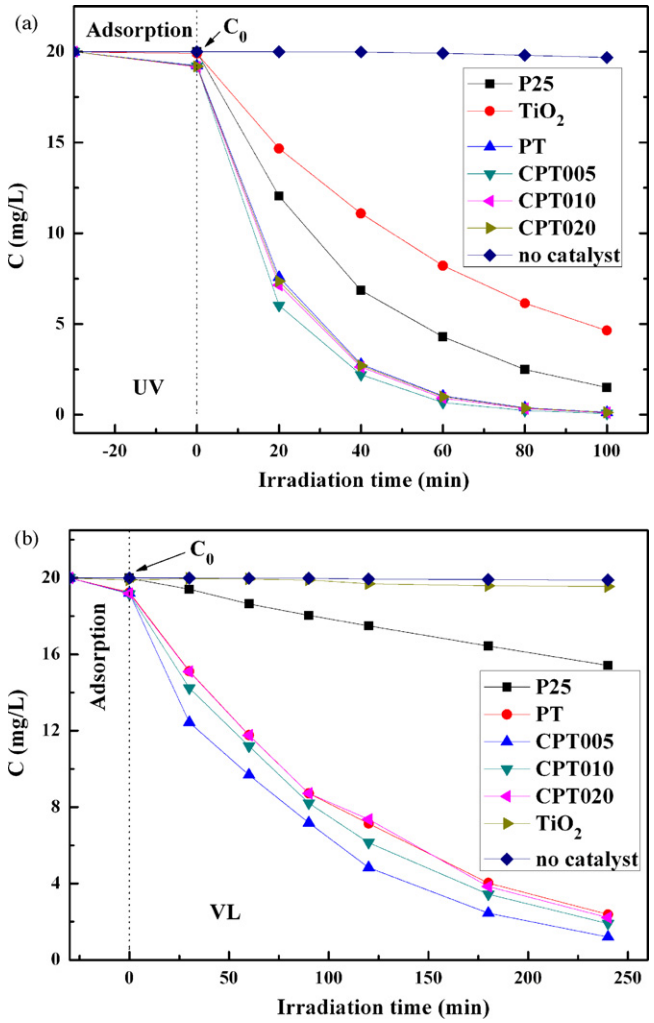


**Fig. 9.** Concentration variation of MO vs. irradiation time in the presence of various catalysts under (a) UV irradiation and (b) VL irradiation.

Fig. 9 shows the photodegradation of MO by the prepared catalysts. About 4% of the MO was adsorbed for PT and CPT composites after stirring for 0.5 h in dark. It increased slightly in comparison with P25 and pure $TiO_2$. The blank experiments of MO degradation without catalyst under the same condition are compared in this study. The blank study indicates that the mere photolysis can be ignored as the corresponding degradation is about 1.6% and 0.5% after illumination for 100 min under UV and for 4 h under VL. Pure $TiO_2$ shows the lowest photactivity, while CPT005 exhibits the highest photocatalytic activity either under UV or under VL irradiation among the prepared **s**amples.

The photocatalytic oxidation of organic contaminants follows roughly the pseudo-first-order reaction kinetics.

$$\ln\left(\frac{C_0}{C}\right) = kKt = k_{app} \times t \text{ or } C_t = C_0 e^{-k_{app}t} \quad (2)$$

where $k_{app}$ is the apparent rate constant, used as the basic kinetic parameter for the different photocatalysts. The initial concentration of MO after achieving adsorption–desorption equilibrium is denoted as $C_0$. The apparent rate constants could be deduced from the linear fitting of $\ln(C_0/C)$ vs. reaction time. The initial degrada-

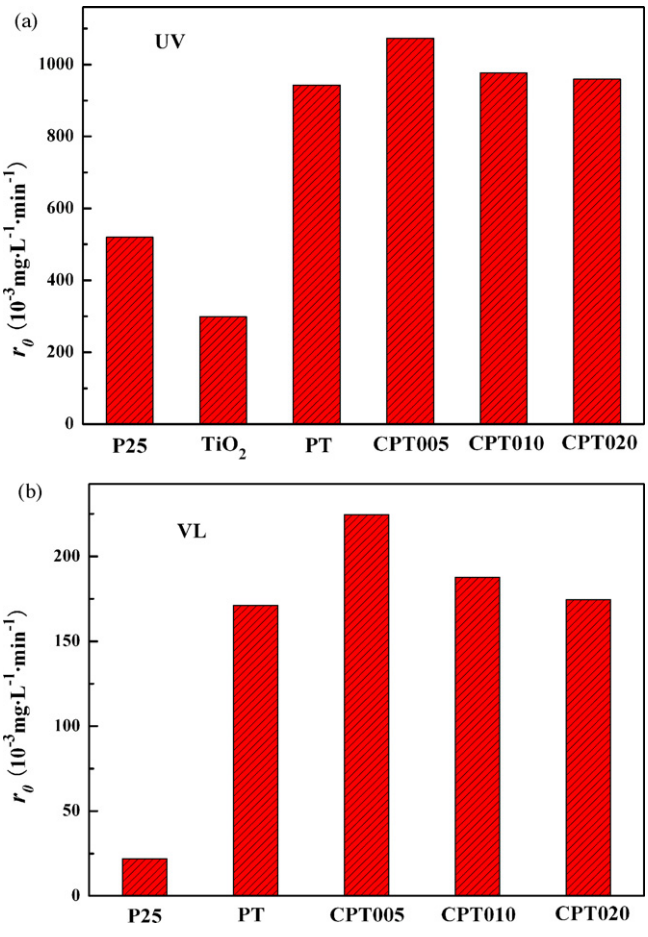


**Fig. 10.** The initial degradation rate of MO in the presence of various catalysts under (a) UV irradiation and (b) VL irradiation.

tion rate ($r_0 = k_{app} \times C_0$) of 20 mg L$^{-1}$ MO with different catalysts was studied and the results are presented in Fig. 10.

The results confirm that $r_0$ is enhanced by P-doping and introducing CNTs. Fig. 10 shows that the activity of PT is higher than that of pure $TiO_2$ under UV illumination. The reason may be that the doped phosphorus is present in the pentavalent-oxidation state, which can replace a part of $Ti^{4+}$ in the crystal lattice of anatase and exist in the form of Ti–O–P bond. Because $P^{5+}$ can accept photoelectron as the electron trap center, its doping reduces the recombination rate of photogenerated charge carriers and increases the photon efficiency. This might explain why the PT sample exhibits higher photocatalytic activity.

A synergetic effect between PT and CNTs on the photocatalytic degradation of MO exists for the composite catalysts. The optimum CNTs/P-$TiO_2$ ratio in the composites is 5% by weight. The decrease in activity with higher CNTs/P-$TiO_2$ weight ratio is considered to be related to the increased absorbing and scattering of photons by surplus carbon in the photoreaction system. The synergetic effect of CNTs on the activity of the composite catalysts may be ascribed to the special structure and performance of CNTs. First, CNTs are eminent electronic conductors that can orderly export excited electron ($e^-$) from conduction band of $TiO_2$ and fleetly reduce electronic accumulation on $TiO_2$ nanoparticles. So the recombination of electron/hole ($e^-/h^+$) pairs could be effectively decreased and thus increase the photon efficiency. Second, because of the large surface areas and different aperture structure, CNTs can adsorb oxygen and dye on the inside or outside surface. Oxygen adsorbed on the surface of CNTs may accept $e^-$ and form $^{\bullet}O_2^-$ which also leads to the formation of $^{\bullet}OH$ in the system. Both $^{\bullet}O_2^-$ and $^{\bullet}OH$ can be responsible for the degradation of the organic compound. Therefore, there are more radicals in the system resulting in the quicker degradation of the dyes. In conclusion, from these two aspects of electron transport and adsorption, CNTs can enhance the effectiveness of azo dye degradation.

While under visible-light irradiation, all CPT samples exhibit higher activity than that of P25. Pure titania shows almost no activity under VL irradiation. This indicates that the presence of a defined amount of CNTs and phosphorus is helpful to improve photocatalytic activity under VL irradiation.

## 4. Conclusions

A new kind of composite photocatalysts by coupling CNTs with phosphorus-doped $TiO_2$ was successfully prepared by hydrothermal method. It is found that the novel CNTs/P-$TiO_2$ photocatalyst has smaller crystalline size, larger surface area and stronger absorption in the visible range than pure $TiO_2$. A synergetic effect on the photocatalytic degradation of MO is observed for the CNTs/P-$TiO_2$ composite catalyst, which exhibits higher photocatalytic activity than P25 and pure $TiO_2$ under both UV and VL irradiation. The surface states of phosphorus allow the more efficient utilization of both UV and visible-light due to the generation of the Ti–O–P linkage in the photocatalyst, and the presence of CNTs promotes the separation of photogenerated carriers. Therefore, adding a suitable amount of CNTs and phosphorus into $TiO_2$ can greatly improve the photocatalytic activity and expand the spectral response range.

## Acknowledgements

We are greatly indebted to the State Ministry of Science and Technology (2008BAE64B05, 2006BAJ04A12-4), the State Key Laboratory of Subtropical Building Science (2008ZA09, 2009ZB05) of China, and the Department of Science and Technology of Guangdong Province (2007A032500005) for their financial support. We also thank Professor Elwood Powell for linguistic correction.

## References

[1] A. Fujishima, K. Honda, Electrochemical photolysis of water at a semiconductor electrode, Nature 238 (1972) 37–38.
[2] A.L. Linsebigler, G. Lu, J.T. Yates, Photocatalysis on $TiO_2$ surfaces: principles, mechanisms, and selected results, Chem. Rev. 95 (1995) 735–758.
[3] O. Legrini, E. Oliveros, A.M. Braun, Photochemical processes for water treatment, Chem. Rev. 93 (1993) 671–698.
[4] M.R. Hoffmann, S.T. Martin, W. Chol, D.W. Bahnemann, Environmental applications of semiconductor photocatalysis, Chem. Rev. 95 (1995) 69–96.
[5] A. Fujishima, T.N. Rao, D.A. Tryk, Titanium dioxide photocatalysis, J. Photochem. Photobiol. C: Photochem. Rev. 1 (2000) 1–21.
[6] R. Asahi, T. Morikawa, T. Ohwaki, K. Aoki, Y. Taga, Visible-light photocatalysis in nitrogen-doped titanium oxides, Science 293 (2001) 269–271.
[7] T. Tachikawa, Y. Takai, S. Tojo, M. Fujitsuka, H. Irie, K. Hashimoto, T. Majima, Visible light-induced degradation of ethylene glycol on nitrogen-doped $TiO_2$ powders, J. Phys. Chem. B 110 (2006) 13158–13165.
[8] Y. Cong, J. Zhang, F. Chen, M. Anpo, Synthesis and characterization of nitrogen-doped $TiO_2$ nanophotocatalyst with high visible light activity, J. Phys. Chem. C 111 (2007) 6976–6982.
[9] S. Somekawa, Y. Kusumoto, M. Ikeda, B. Ahmmad, Y. Horie, Fabrication of N-doped $TiO_2$ thin films by laser ablation method: mechanism of N-doping and evaluation of the thin films, Catal. Commun. 9 (2008) 437–440.
[10] W. Zhao, W. Ma, C. Chen, J. Zhao, Z. Shuai, Efficient degradation of toxic organic pollutants with $Ni_2O_3/TiO_2$–*x*B*x* under visible irradiation, J. Am. Chem. Soc. 126 (2004) 4782–4783.
[11] S.U.M. Khan, M. Al-Shahry, W.B. Ingler, Efficient photochemical water splitting by a chemically modified n-$TiO_2$, Science 297 (2002) 2243–2245.
[12] M.S. Wong, S.W. Hsu, K.K. Rao, C.P. Kumar, Influence of crystallinity and carbon content on visible light photocatalysis of carbon doped titania thin films, J. Mol. Catal. A 279 (2008) 20–26.
[13] Y. Xie, X.J. Zhao, The effects of synthesis temperature on the structure and visible-light-induced catalytic activity of F–N-codoped and S–N-codoped titania, J. Mol. Catal. A 285 (2008) 142–149.
[14] T. Umebayashi, T. Yamaki, H. Itoh, K. Asai, Band gap narrowing of titanium dioxide by sulfur doping, Appl. Phys. Lett. 81 (2002) 454–456.

[15] D. Li, H. Haneda, S. Hishita, N. Ohashi, Visible-light-driven N–F-codoped $TiO_2$ photocatalysts. 1. Synthesis by spray pyrolysis and surface characterization, Chem. Mater. 17 (2005) 2588–2595.
[16] J.C. Yu, L. Zhang, Z. Zheng, J. Zhao, Synthesis and characterization of phosphated mesoporous titanium dioxide with high photocatalytic activity, Chem. Mater. 15 (2003) 2280–2286.
[17] H. Luo, T. Takata, Y. Lee, J. Zhao, K. Domen, Y.S. Yan, Photocatalytic activity enhancing for titanium dioxide by co-doping with bromine and chlorine, Chem. Mater. 16 (2004) 846–849.
[18] L. Lin, W. Lin, Y.X. Zhu, B.Y. Zhao, Y.C. Xie, Phosphor-doped titania–a novel photocatalyst active in visible light, Chem. Lett. 34 (2005) 284–285.
[19] Q. Shi, D. Yang, Z. Jiang, J. Li, Visible-light photocatalytic regeneration of NADH using P-doped $TiO_2$ nanoparticles, J. Mol. Catal. B 43 (2006) 44–48.
[20] L. Korosi, A. Oszko, G. Galbacs, A. Richardt, V. Zollmer, I. Dekany, Structural properties and photocatalytic behavior of phosphate-modified nanocrystalline titania films, Appl. Catal. B 77 (2007) 175–183.
[21] L. Korosi, S. Papp, I. Bertoti, I. Dekany, Surface and bulk composition, structure, and photocatalytic activity of phosphate-modified $TiO_2$, Chem. Mater. 19 (2007) 4811–4819.
[22] H. Ozaki, N. Fujimoto, S. Iwamoto, M. Inoue, Photocatalytic activities of $NH_3$-treated titania modified with other elements, Appl. Catal. B 70 (2007) 431–436.
[23] L. Lin, W. Lin, J.L. Xie, Y.X. Zhu, B.Y. Zhao, Y.C. Xie, Photocatalytic properties of phosphor-doped titania nanoparticles, Appl. Catal. B 75 (2007) 52–58.
[24] R. Zheng, L. Lin, J. Xie, Y. Zhu, Y. Xie, State of doped phosphorus and its influence on the physicochemical and photocatalytic properties of P-doped titania, J. Phys. Chem. C 112 (2008) 15502–15509.
[25] C. Jin, R.Y. Zheng, Y. Guo, J.L. Xie, Y.X. Zhu, Y.C. Xie, Hydrothermal synthesis and characterization of phosphorous-doped $TiO_2$ with high photocatalytic activity for methylene blue degradation, J. Mol. Catal. A 313 (2009) 44–48.
[26] J. Matos, J. Laine, J.M. Herrmann, Synergy effect in the photocatalytic degradation of phenol on a suspended mixture of titania and activated carbon, Appl. Catal. B 18 (1998) 281–291.
[27] S.X. Liu, X.Y. Chen, X. Chen, A $TiO_2$/AC composite photocatalyst with high activity and easy separation prepared by a hydrothermal method, J. Hazard. Mater. 143 (2007) 257–263.
[28] X.J. Wang, Y.F. Liu, Z.H. Hu, Y.J. Chen, W. Liu, G.H. Zhao, Degradation of methyl orange by composite photocatalysts nano-$TiO_2$ immobilized on activated carbons of different porosities, J. Hazard. Mater. 169 (2009) 1061–1067.
[29] L.W. Zhang, H.B. Fu, Y.F. Zhu, Efficient $TiO_2$ photocatalysts from surface hybridization of $TiO_2$ particles with graphite-like carbon, Adv. Funct. Mater. 18 (2008) 2180–2189.
[30] Z.B. Lei, Y. Xiao, L.Q. Dang, W.S. You, G.S. Hu, J. Zhang, Nickel-catalyzed fabrication of $SiO_2$, $TiO_2$/graphitized carbon, and the resultant graphitized carbon with periodically macroporous structure, Chem. Mater. 19 (2007) 477–484.
[31] Y. Yu, J.C. Yu, C.Y. Chan, Y.K. Che, J.C. Zhao, L. Ding, W.K. Ge, P.K. Wong, Enhancement of adsorption and photocatalytic activity of $TiO_2$ by using carbon nanotubes for the treatment of azo dye, Appl. Catal. B 61 (2005) 1–11.
[32] C.Y. Kuo, Prevenient dye-degradation mechanisms using UV/$TiO_2$/carbon nanotubes process, J. Hazard. Mater. 163 (2009) 239–244.
[33] S. Sakthivel, H. Kisch, Daylight photocatalysis by carbon-modified titanium dioxide, Angew. Chem. Int. Ed. 42 (2003) 4908–4911.
[34] J.L. Faria, W.D. Wang, Carbon materials in photocatalysis, in: P. Serp, J.L. Figueiredo (Eds.), Carbon Materials for Catalysis, vol. 579, John Wiley & Sons, 2008.
[35] P. Serp, M. Corrias, P. Kalck, Carbon nanotubes and nanofibers in catalysis, Appl. Catal. A 253 (2003) 337–358.
[36] W.D. Wang, P. Serp, P. Kalck, J.L. Faria, Photocatalytic degradation of phenol on MWNT and titania composite catalysts prepared by a modified sol–gel method, Appl. Catal. B 56 (2005) 305–312.
[37] Y. Yao, G.H. Li, S. Ciston, R.M. Lueptow, K.A. Gray, Photoreactive $TiO_2$/carbon nanotube composites: synthesis and reactivity, Environ. Sci. Technol. 42 (2008) 4952–4957.
[38] B. Liu, H.C. Zeng, Carbon nanotubes supported mesoporous mesocrystals of anatase $TiO_2$, Chem. Mater. 20 (2008) 2711–2718.
[39] G.M. An, W.H. Ma, Z.Y. Sun, Z.M. Liu, B.X. Han, S.D. Miao, Z.J. Miao, K.L. Ding, Preparation of titania/carbon nanotube composites using supercritical ethanol and their photocatalytic activity for phenol degradation under visible light irradiation, Carbon 45 (2007) 1795–1801.
[40] C.Y. Yen, Y.F. Lin, C.H. Hung, Y.H. Tseng, C.C. Ma, M.C. Chang, H. Shao, The effects of synthesis procedures on the morphology and photocatalytic activity of multi-walled carbon nanotubes/$TiO_2$ nanocomposites, Nanotechnology 19 (2008) 1–11.
[41] B. Gao, G.Z. Chen, G.L. Puma, Carbon nanotubes/titanium dioxide (CNTs/$TiO_2$) nanocomposites prepared by conventional and novel surfactant wrapping sol–gel methods exhibiting enhanced photocatalytic activity, Appl. Catal. B: Environ. 89 (2009) 503–509.
[42] M.S.P. Shaffer, X. Fan, A.H. Windle, Dispersion and packing of carbon nanotubes, Carbon 36 (1998) 1603–1612.
[43] C. Peng, G.A. Snook, D.J. Fray, M.S.P. Shaffer, G.Z. Chen, Carbon nanotube stabilized emulsions for electrochemical synthesis of porous nanocomposite coatings of poly[3,4-ethylene-dioxythiophene], Chem. Commun. 44 (2006) 4629–4631.
[44] Z. Song, J. Hrbek, R. Osgood, Formation of $TiO_2$ nanoparticles by reactive-layer-assisted deposition and characterization by XPS and STM, Nano Lett. 5 (2005) 1327–1332.
[45] J.C. Yu, W. Ho, J. Yu, H. Yip, P.K. Wong, J. Zhao, Efficient visible-light-induced photocatalytic disinfection on sulfur-doped nanocrystalline titania, Environ. Sci. Technol. 39 (2005) 1175–1179.
[46] Y.B. Xie, C.W. Yuan, Visible-light responsive cerium ion modified titania sol and nanocrystallites for X-3B dye photodegradation, Appl. Catal. B: Environ. 46 (2003) 251–259.
[47] K.E. Kim, K.J. Kim, W.S. Jung, S.Y. Bae, J. Park, J. Choi, J. Choo, Investigation on the temperature-dependent rate of carbon nanotubes using chemical vapor deposition of ferrocene and acetylene, Chem. Phys. Lett. 401 (2005) 459–464.
[48] K. Yang, Y. Dai, B. Huang, Understanding photocatalytic activity of S- and P-doped $TiO_2$ under visible light from first-principles, J. Phys. Chem. C 111 (2007) 18985–18994.